PARKINSON'S DISEASE

GPNMB confers risk for Parkinson's disease through interaction with α-synuclein

Maria E. Diaz-Ortiz†, Yunji Seo†, Marijan Posavi, Marc Carceles Cordon, Elisia Clark, Nimansha Jain, Rakshita Charan, Michael D. Gallagher, Travis L. Unger, Noor Amari, R. Tyler Skrinak, Roseanne Davila-Rivera, Eliza M. Brody, Noah Han, Rebecca Zack, Vivianna M. Van Deerlin, Thomas F. Tropea, Kelvin C. Luk, Edward B. Lee, Daniel Weintraub, Alice S. Chen-Plotkin*

INTRODUCTION: An estimated 6 million people worldwide are affected by Parkinson's disease (PD), for which there are no disease-modifying therapies. Since 2005, genome-wide association studies (GWASs) have aimed to find common variant risk loci for PD. These PD GWASs have now uncovered 90 genome-wide significant risk signals. However, target genes and mechanisms remain largely unknown, hampering the field's ability to develop downstream therapeutic approaches from these genomic studies.

RATIONALE: We dissected a chromosome 7 locus linked to risk for PD by GWASs to find the target gene and understand its role in PD pathophysiology. We first performed colocalization analyses of expression quantitative trait locus (eQTL) and PD risk signals, confirming eQTL effects with allele-specific expression (ASE) studies of candidate target genes in the human brain. We then characterized the consequences of manipulating target gene expression in human induced pluripotent stem cell–derived neurons (iPSC-Ns) and other cell models. Finally, we determined whether levels of the target gene or protein were associated with disease state and severity in humans.

RESULTS: We linked the GWAS-derived chromosome 7 PD risk locus [sentinel single-nucleotide polymorphism (SNP) rs199347] to *GPNMB*—which encodes the transmembrane protein glycoprotein nonmetastatic melanoma protein B (GPNMB)—with a 94% posterior probability of the PD risk and caudate *GPNMB* eQTL signals sharing a causal variant. In human brain samples across multiple brain regions (the caudate, cerebellum, and cingulate cortex) from both PD cases (n = 4) and neurologically normal controls (n = 2), ASE studies confirmed that the PD risk–associated haplotype was associated with threefold higher *GPNMB* expression.

Having linked *GPNMB* expression levels to PD risk, we generated iPSC-N lines with normal levels of *GPNMB* [wild-type (WT)], heterozygous loss of *GPNMB* (Het), or homozygous loss of *GPNMB* [knockout (KO); two different lines generated] by CRISPR-Cas9 genome editing. Analyzing these iPSC-Ns using confocal microscopy, we found that loss of *GPNMB* was accompanied by a marked reduction in α-synuclein (aSyn) at the synapse—a result confirmed by immunoblotting of synaptosomal preparations for aSyn. Culturing the iPSC-Ns for an additional week, to a state of greater maturity, only exaggerated the differences in synaptic aSyn when comparing WT versus all other lines. Moreover, transcriptomic profiling of these genome-edited iPSC-N lines revealed that aSyn served as a key protein-protein interaction hub for genes with dysregulated expression in *GPNMB* Het and KO states.

Because aSyn is the protein that accumulates in the hallmark pathological inclusions of PD, and because progression of PD may result from the uptake and cell-to-cell spread of pathological forms of aSyn, we further explored the relationship between GPNMB and aSyn. In HEK293 and HeLa cells, we found that GPNMB and aSyn colocalized and coimmunoprecipitated. In iPSC-Ns, we observed minimal uptake of fibrillar forms of aSyn in *GPNMB* Het and KO iPSC-Ns, in contrast to rapid and obvious uptake of fibrillar aSyn by WT iPSC-Ns. Additionally, when iPSC-Ns were cultured for 14 days after a one-time addition of fibrillar aSyn to the culture medium, WT iPSC-Ns developed hyperphosphorylated, insoluble inclusions of aSyn, but these forms of aSyn pathology were minimal in *GPNMB* Het and KO iPSC-Ns. These experiments, together, demonstrated that GPNMB was necessary for internalization of fibrillar aSyn and subsequent development of aSyn pathology. Meanwhile, in cell lines with low *GPNMB* expression that do not normally internalize fibrillar aSyn, exogenous expression of *GPNMB* was sufficient to confer ability to take up aSyn. Finally, using samples from 731 PD and 59 neurologically normal control individuals, we found that plasma GPNMB is elevated in PD and that PD individuals with higher plasma GPNMB levels have more severe disease.

CONCLUSION: Computational, cell biological, and human tissue–based studies establish *GPNMB* as a GWAS-derived risk gene for PD, with higher expression levels mediating pathogenicity through interactions with aSyn. As a transmembrane protein that is expressed at the cell surface, with an extracellular, soluble form generated by cleavage, GPNMB is a candidate for biomarker development and therapeutic targeting in PD. ∎
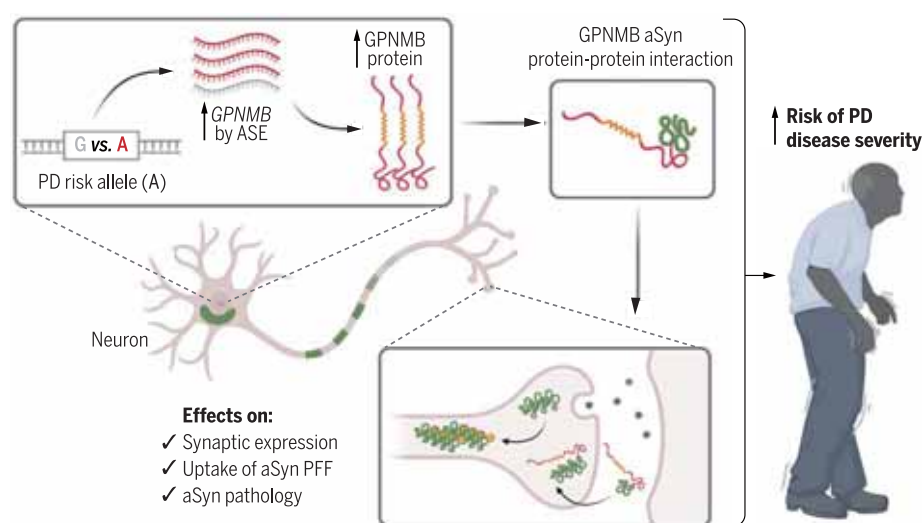
GPNMB and aSyn in PD. Haplotypes associated with PD result in increased expression of *GPNMB*, encoding GPNMB. GPNMB interacts with aSyn, with effects on aSyn expression at the synapse, cellular uptake of fibrillar aSyn, and development of aSyn pathology in neurons. Together, these cellular processes mediate risk for development and progression of PD. Created with BioRender.com. PFF, preformed fibril.

READ THE FULL ARTICLE AT
https://doi.org/10.1126/science.abk0637

PARKINSON'S DISEASE

GPNMB confers risk for Parkinson's disease through interaction with α-synuclein

Maria E. Diaz-Ortiz[1,2]†, Yunji Seo[1]†, Marijan Posavi[1], Marc Carceles Cordon[1], Elisia Clark[1], Nimansha Jain[1,3], Rakshita Charan[1,4], Michael D. Gallagher[1,5], Travis L. Unger[1], Noor Amari[1], R. Tyler Skrinak[1], Roseanne Davila-Rivera[1], Eliza M. Brody[1], Noah Han[1], Rebecca Zack[1], Vivianna M. Van Deerlin[6], Thomas F. Tropea[1], Kelvin C. Luk[6], Edward B. Lee[6], Daniel Weintraub[7,8], Alice S. Chen-Plotkin[1]*

Many risk loci for Parkinson's disease (PD) have been identified by genome-wide association studies (GWASs), but target genes and mechanisms remain largely unknown. We linked the GWAS-derived chromosome 7 locus (sentinel single-nucleotide polymorphism rs199347) to *GPNMB* through colocalization analyses of expression quantitative trait locus and PD risk signals, confirmed by allele-specific expression studies in the human brain. In cells, glycoprotein nonmetastatic melanoma protein B (GPNMB) coimmunoprecipitated and colocalized with α-synuclein (aSyn). In induced pluripotent stem cell–derived neurons, loss of *GPNMB* resulted in loss of ability to internalize aSyn fibrils and develop aSyn pathology. In 731 PD and 59 control biosamples, GPNMB was elevated in PD plasma, associating with disease severity. Thus, *GPNMB* represents a PD risk gene with potential for biomarker development and therapeutic targeting.

P arkinson's disease (PD) is a progressive neurodegenerative disease affecting an estimated 5 million people worldwide (*1*). Although genome-wide association studies (GWASs) have nominated >80 genetic loci as PD risk factors (*2*), target genes and mechanisms for these loci remain largely unknown. To date, drug development in PD has focused on pathways related to α-synuclein (aSyn)—the main component of disease-defining neuropathological lesions—or a handful of other genes causal for PD in a small minority of patients (*3*, *4*). However, these efforts have not yet yielded successful disease-modifying therapies.

In this work, we sought to widen the net for PD therapeutic targets by dissecting a common variant GWAS-derived PD risk locus. We used computational, cell biological, and human tissue–based approaches to ascertain that *GPNMB* is a bona fide PD risk gene. Moreover, we implicated glycoprotein nonmetastatic melanoma protein B (GPNMB)–aSyn interactions and GPNMB expression levels in the development of PD.

GPNMB is the target gene at the rs199347 PD risk locus

Multiple GWASs have linked a chromosome 7 locus [sentinel single-nucleotide polymorphism (SNP) rs199347] with PD (*2*, *5*). Because rs199347 and linked variants are noncoding, we hypothesized that this locus confers PD risk through the modulation of expression levels of one or more target genes, as has been shown for a number of common variant GWAS-derived risk factors in other diseases (*6–9*). To nominate candidate target genes, we used the Genotype Tissue Expression (GTEx) database (*10*), finding genes for which a shared causal variant could be linked to both PD risk and expression levels in normal human tissue. Target genes within a 1-Mb window of the sentinel SNP were evaluated in colocalization analyses (*11*, *12*): *GPNMB*, *KLHL7*, and *NUPL2* (fig. S1). Among these, *GPNMB* demonstrated the greatest overlap between PD risk and expression quantitative trait locus (eQTL) effects, with the most significant colocalization effects seen in the PD-affected caudate brain region (fig. S1B). Moreover, when we examined eQTL effects more broadly, we found that rs199347 genotypes associated significantly with *GPNMB* expression levels in all GTEx-characterized brain regions as well as in whole blood (Fig. 1A). Thus, computational analyses of existing databases strongly implicated *GPNMB* as the target gene at this locus, with higher levels of brain and blood expression linked to PD risk.

The mechanistic basis for eQTL effects lies in allele-specific expression (ASE), whereby different alleles at a given locus show different levels of expression (*13*). Thus, to validate the database-predicted eQTL relationship between rs199347 and *GPNMB* expression, we developed a capture RNA sequencing (RNA-seq)–based (*14*) ASE assay for human brain tissue (Fig. 1B) and used it to investigate whether individuals carrying two different alleles for the rs199347 haplotype demonstrated ASE for *GPNMB*. Moreover, to understand whether rs199347 haplotype effects on brain tissue expression extended to PD brains, we characterized multiple brain regions with varying degrees of pathological involvement in PD (in order of greatest to least aSyn pathological involvement: the caudate, cingulate, and cerebellum) from both PD cases (*n* = 4) and neurologically normal controls (NCs) (*n* = 2; extended demographic information is available in table S1).

We found a high degree of ASE for *GPNMB* regardless of PD status or brain region, with 15 of 15 brain samples showing significant ASE (Fig. 1C). Moreover, all samples displayed the same direction of effect, with the PD risk haplotype associating with higher expression levels, averaging approximately threefold higher than the PD protective haplotype. By contrast, ASE analyses for another gene at this locus, *KLHL7*, did not show preferential expression of either haplotype (Fig. 1C). Finally, we confirmed that GPNMB is expressed at the protein level in the human brain, examining multiple postmortem cases (table S1) by immunoblotting (Fig. 1D), which demonstrated a main band at the predicted molecular weight of 72 kD across all cases, as well as a variably expressed higher–molecular weight band that collapses to 72 kD with deglycosylation (fig. S2), consistent with prior accounts of GPNMB's variably glycosylated forms (*15*). To better understand what cell types might be expressing GPNMB, we also performed immunohistochemical staining of human brain tissue (Fig. 1E and table S1) and found GPNMB expression in multiple cell types, consistent with studies of spinal cord tissue (*16*). Thus, both database-predicted and empirically validated eQTL studies in human PD samples support *GPNMB* as the target gene at the rs199347 locus, with protein expression in the brain.

## Loss of GPNMB in iPSC-Ns decreases synaptic aSyn

Having nominated *GPNMB* as the mechanistic link between a GWAS locus and PD risk, we sought to define its function in a disease-relevant context. *GPNMB* encodes the GPNMB protein, a transmembrane glycoprotein first identified in a screen of human melanoma cells with varying potential for metastasis (*17*). Although GPNMB has subsequently been

[1]Department of Neurology, Perelman School of Medicine, University of Pennsylvania, Philadelphia, PA, USA. [2]Department of Bioengineering, School of Engineering and Applied Sciences, University of Pennsylvania, Philadelphia, PA, USA. [3]Department of Neurology, Hope Center for Neurological Disorders, Knight Alzheimer Disease, Research Center, Washington University, St. Louis, MO, USA. [4]Flagship Pioneering, Cambridge, MA, USA. [5]Whitehead Institute for Biomedical Research, Cambridge, MA, USA. [6]Center for Neurodegenerative Disease Research, Department of Pathology and Laboratory Medicine, Perelman School of Medicine, University of Pennsylvania, Philadelphia, PA, USA. [7]Department of Psychiatry, Perelman School of Medicine, University of Pennsylvania, Philadelphia, PA, USA. [8]Parkinson's Disease Research, Education and Clinical Center (PADRECC), Corporal Michael J. Crescenz VA Medical Center, Philadelphia, PA, USA.
*Corresponding author. Email: chenplot@pennmedicine.upenn.edu
†These authors contributed equally to this work.
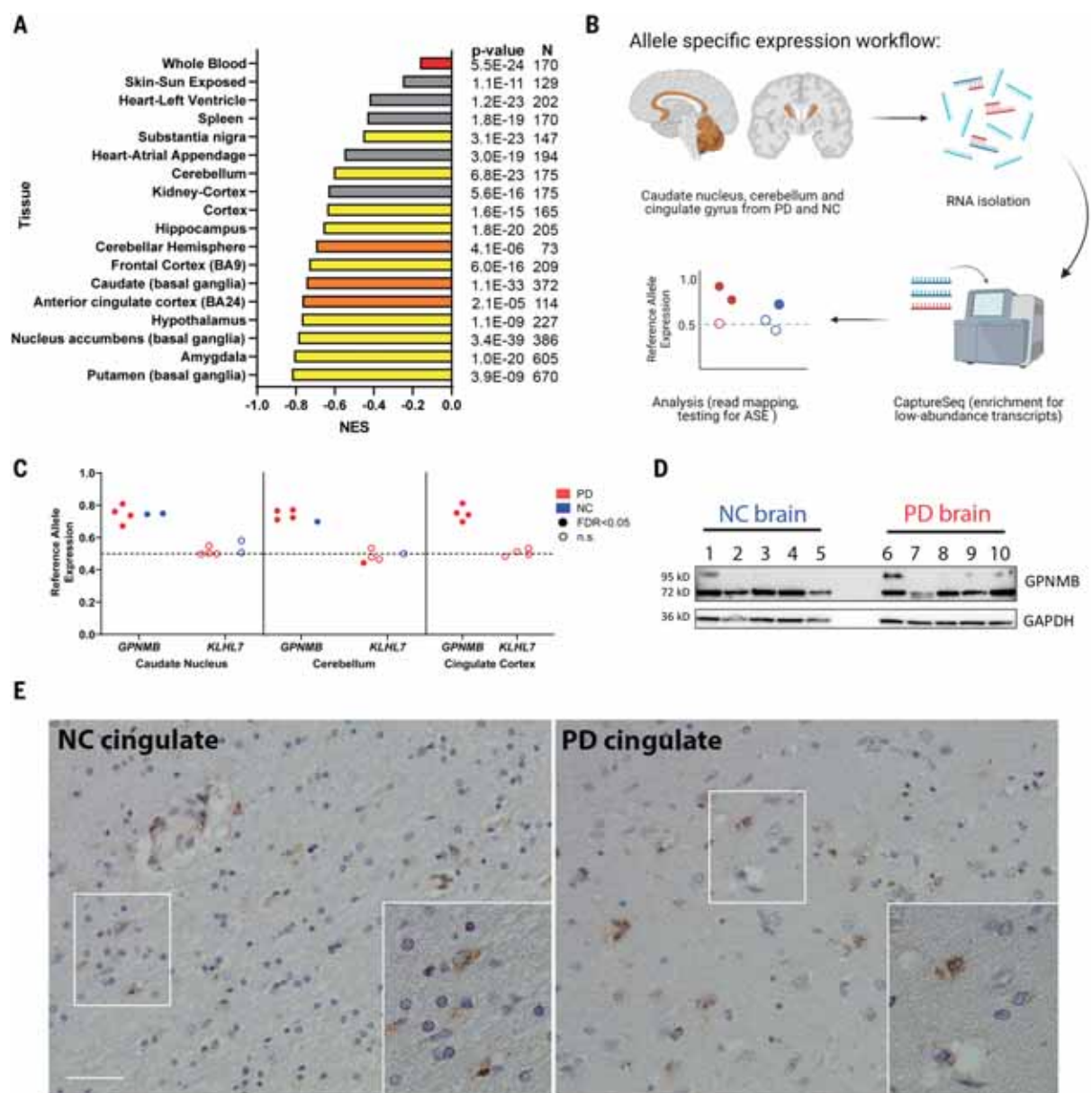
Fig. 1. Chromosome 7 PD risk locus is a multitissue *GPNMB* eQTL and shows ASE. (**A**) GTEx normalized expression size (NES) coefficients for rs199347's effect on *GPNMB* expression in various tissues (*10*). Red indicates whole blood, and yellow and orange indicate brain regions. Orange bars correspond to brain regions analyzed for ASE. The PD risk allele at rs199347 (allele = A) is uniformly associated with higher *GPNMB* mRNA expression. (**B**) Workflow for ASE experiment in brain samples from PD patients (*n* = 4) and NCs (*n* = 2). (**C**) ASE analysis for rs199347 target gene candidates *GPNMB* and *KLHL7* in caudate, cerebellum, and cingulate cortex brain samples of PD (red) and NC (blue) individuals heterozygous at this locus. Shaded dots indicate significant (Benjamini-Hochberg–adjusted $P < 0.05$) ASE, whereas empty dots do not show significant ASE. In the absence of ASE, the allelic ratio would be 0.5. For *GPNMB*, the allelic ratio approached 0.8, with higher expression for the *GPNMB* allele carrying the PD risk haplotype. n.s., not significant. (**D**) Immunoblots showing GPNMB expression in caudate brain lysates from NC (*n* = 5) and PD (*n* = 5) individuals. A 72-kD band was detected by the E1Y7J antibody in all cases, with variable expression of a higher–molecular weight glycosylated form. A glyceraldehyde-3-phosphate dehydrogenase (GAPDH) loading control is also shown. (**E**) Representative immunohistochemical staining of GPNMB in NC and PD brains demonstrates expression in multiple cell types. Scale bar, 50 μm.

found to enhance malignant phenotypes in a number of cancers (*18*), characterization of its function in the brain or in neurons is scant (*15*, *16*, *19–21*). We thus turned to a rapidly inducible human induced pluripotent stem cell–derived cortical neuron (iPSC-N) model (*22*) in which we could directly manipulate *GPNMB* levels to investigate its neuronal function.

Using CRISPR-Cas9 genome editing, we generated iPSC-N lines with normal levels of *GPNMB* [wild-type (WT)], heterozygous loss of *GPNMB* (Het), or homozygous loss of *GPNMB* [two lines: knockout 1 (KO1) and KO2; figs. S3 and S4] and assessed them by confocal microscopy. At a time point when morphology, expression of neuronal markers, and ability to fire trains of action potentials reportedly indicate maturity [14 days after neuronal induction (*22*)], loss of *GPNMB* was accompanied by a marked reduction in aSyn at the synapse (Fig. 2, A and B). Moreover, similar levels of decrease were observed in the Het, KO1, and KO2 lines when we quantified microscopy results (Fig. 2C). By contrast, staining
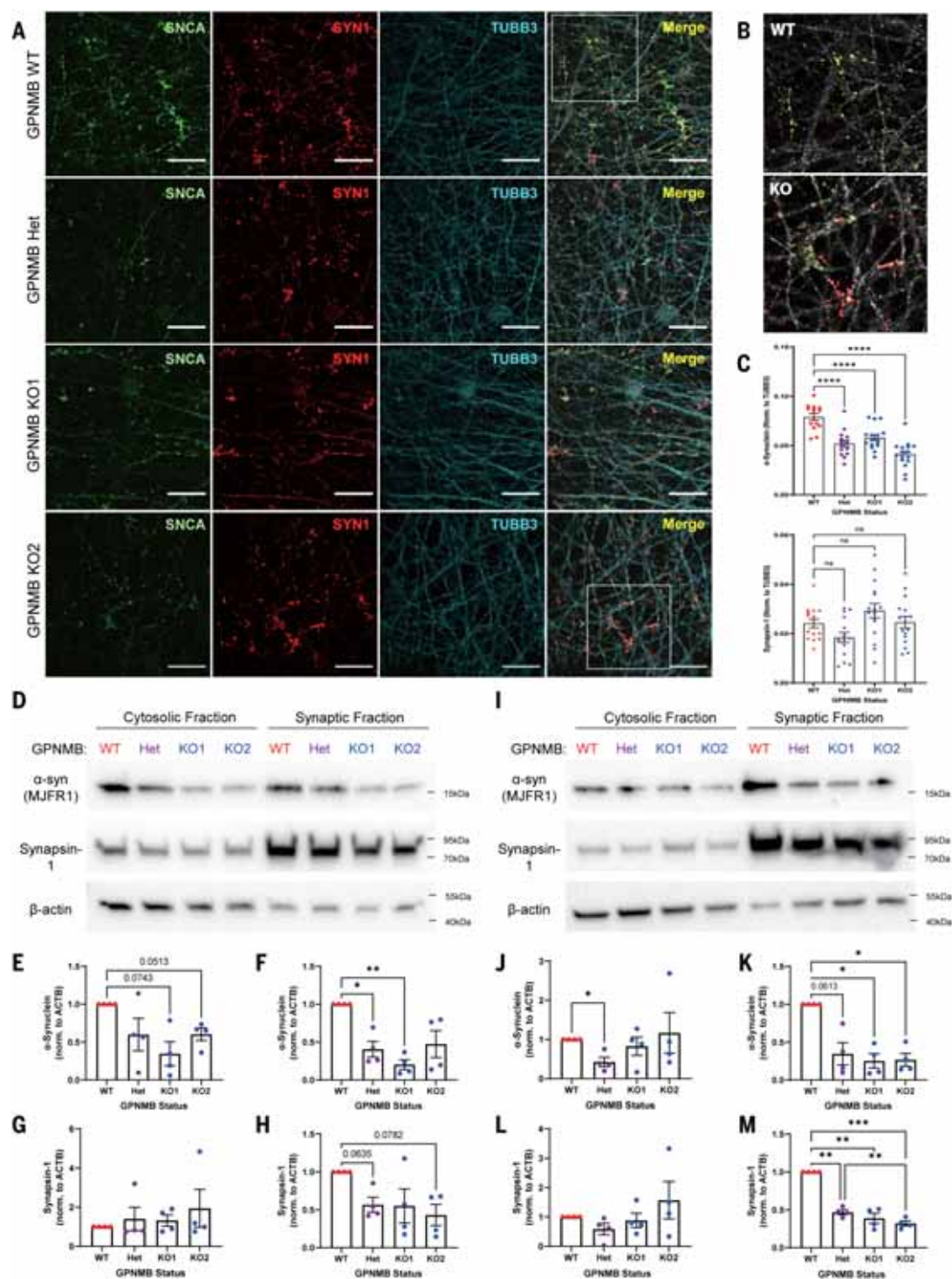
Fig. 2. Heterozygous and homozygous loss of GPNMB results in altered aSyn expression and localization. (**A**) Immunofluorescence imaging of aSyn (SNCA, green, stained with MJFR1 antibody), synapsin-1 (SYN1, red), and β-tubulin (TUBB3, cyan) in GPNMB WT, Het, KO1, and KO2 iPSC-Ns acquired 14 days after induction of neuronal differentiation. Scale bars, 20 μm. (**B**) 2× magnified images of merged insets from (A) demonstrate greatly reduced localization of aSyn (SNCA, green) to synapses (labeled with SYN1, red) in GPNMB KO iPSC-Ns compared with WT. TUBB3 is converted to gray. (**C**) Quantification of aSyn (top) and synapsin-1 (bottom). N = 15 images (five images from each of three wells) per condition. Means ± SEMs, as well as individual data points, are shown. Statistics are by one-way ANOVA followed by post hoc Dunnett's test comparing all other groups to WT. ns = P > 0.05; ****P < 0.0001. (**D** and **I**) Western blots showing cytosolic and synaptosomal expression of aSyn, synapsin-1, and β-actin in iPSC-N lysates isolated at day 14 (D) and day 21 (I) after neuronal induction. (**E** to **H**) Quantification of day 14 immunoblots for either aSyn [(E) and (F)] or synapsin-1 [(G) and (H)] expression in the cytosolic [(E) and (G)] or synaptosomal [(F) and (H)] fractions. (**J** to **M**) Quantification of day 21 immunoblots for aSyn [(J) and (K)] or synapsin-1 [(L) and (M)] expression in the cytosolic [(J) and (L)] or synaptosomal [(K) and (M)] fractions. N = 4 blots per time point from four independent differentiations. Means ± SEMs, as well as individual data points, are shown. Statistics are by one-way ANOVA with repeated measures followed by post hoc Tukey test. *P < 0.05; **P < 0.01; ***P < 0.001.

of synapsin-1, another presynaptic terminal protein, did not differ significantly among the iPSC-N lines (Fig. 2C).

To corroborate our immunofluorescence findings, we isolated synaptosomes from the WT, Het, KO1, and KO2 iPSC-N lines and quantified aSyn by immunoblot in both the synaptosomal and cytosolic fractions (Fig. 2, D to M). At the same time point as our microscopy experiments, synaptosomal aSyn was decreased in the Het and KO1 lines (Fig. 2, D and F). By contrast, neither synaptosomal nor cytosolic synapsin-1 levels differed significantly among the WT, Het, KO1, and KO2 lines (Fig. 2, G and H).

Because aSyn expression at the synapse increases as neurons mature (23, 24), we investigated whether the observed loss of aSyn could be the result of a delay in neuronal maturation that would improve over time. However, after an additional week of neuronal differentiation, differences in aSyn only increased, with the *GPNMB* Het, KO1, and KO2 lines showing ~75% reduction in the synaptosomal aSyn fraction compared with the WT line (Fig. 2, I and K). In addition, by 21 days after induction, both aSyn and synapsin-1 were found primarily in the synaptosomal fraction, and synapsin-1 levels were also significantly decreased in the *GPNMB* Het, KO1, and KO2 lines compared with the WT line (Fig. 2M).

Thus, decreased expression of *GPNMB* in neurons leads to loss of aSyn at the synapse, which suggests direct links between the rs199347 risk haplotype, *GPNMB* expression, and aSyn. Moreover, loss of *GPNMB* may result in a broader synaptic defect.

Transcriptomic profiling of iPSC-Ns reveals *GPNMB* effects on synaptic biology and aSyn

To obtain an unbiased view of biological changes induced by loss of *GPNMB* in neurons, we transcriptionally profiled five independent replicates each of the *GPNMB* WT, Het, and KO2 (hereafter referred to as just KO) iPSC-N lines. Although all three lines showed similar gene expression at baseline, upon neuronal differentiation, distinct profiles emerged for the WT versus the Het and KO cells (fig. S5). Specifically, regardless of whether we performed hierarchical clustering using the top 35 differentially expressed genes (Fig. 3A and fig. S5) or principal components analysis (PCA) using all expressed genes (Fig. 3B and fig. S5), *GPNMB* WT lines separated from the Het and KO lines, whereas within-line replicates clustered together. As expected, across all cell lines, as neuronal differentiation occurred, neuronal genes (e.g., *MAP2*, *TUBB3*, and *SYN1*) were up-regulated, whereas pluripotency genes (e.g., *SOX2*) were downregulated (fig. S6).

In the neuronally differentiated lines, overlap among genes dysregulated in the *GPNMB* Het and *GPNMB* KO lines compared with the WT line was considerable, with 142 and 449 overlapping up-regulated and down-regulated genes, respectively (out of 177 and 610 up- and down-regulated genes, respectively, in the Het condition, and 176 and 525 up- and down-regulated genes, respectively, in the KO condition). By contrast, relatively few genes showed differential expression comparing the *GPNMB* Het versus KO lines (Fig. 3, C to E).

Globally, two modules of coexpressed genes distinguished WT from *GPNMB* Het and KO iPSC-Ns, with one module (M1) increased in expression in WT compared with *GPNMB* Het and KO iPSC-Ns and one module (M2) decreased in expression in WT iPSC-Ns (fig. S5). Biological pathway analysis of M1 genes revealed a highly significant overrepresentation of synapse-related categories (Fig. 3F and table S2), corroborating our cell biological findings. The top three categories overrepresented in M2 genes related to receptor tyrosine kinases (Fig. 3G and table S3).

Using module coexpression network analysis with the GeneMANIA (25) database of protein-protein interactions (Fig. 3, H and I), we found that aSyn (encoded by *SNCA*) served as a key protein-protein interaction hub for M1 genes with dysregulated expression in *GPNMB* Het and KO states. These data—from unbiased bottom-up analyses of global gene expression—highlight the strong functional effects of *GPNMB* loss on aSyn.

GPNMB is necessary and sufficient for cellular internalization of aSyn

Because data from the edited iPSC-N lines supported a functional interaction between GPNMB and aSyn from both targeted and unbiased lines of investigation, we investigated whether these two proteins might directly interact. In iPSC-Ns, *GPNMB* expression is not high, which makes visualization and co-immunoprecipitation (co-IP) experiments challenging, so we began with immortalized cell lines. Confocal microscopy of GPNMB and aSyn revealed colocalization between GPNMB and aSyn in LAMP1+ cytoplasmic punctae when transfected in both HeLa (Fig. 4A) and HEK293 (fig. S2) cells. Moreover, when expressed in both cell types, GPNMB and aSyn coimmunoprecipitated, regardless of whether the immunoprecipitated protein was GPNMB or aSyn (Fig. 4, B and C, and fig. S2).

Encouraged by these data that suggest that a GPNMB-aSyn protein-protein interaction might form the basis for the profound effects on aSyn caused by loss of *GPNMB*, we next investigated the functional interaction of these two proteins in a cellular model of PD. Specifically, when aSyn is fibrillized and introduced in the culture medium to neurons, including iPSC-Ns, these fibrillar forms of aSyn are known to be internalized by the cells, which will subsequently develop aSyn inclusions with pathological hallmarks, including phosphorylation at serine 129 (S129) and decreased solubility (26). We thus used this PD model to probe the effects of neuronal loss of *GPNMB* by introducing fibrillar aSyn to cultures of our *GPNMB* WT, Het, and KO iPSC-Ns.

Although WT iPSC-Ns at a mature stage of differentiation readily internalized labeled preformed fibrils (PFFs) of aSyn (Fig. 4D, second row), we observed a significant reduction in aSyn internalization in the Het and KO iPSC-N lines, to levels barely above background (Fig. 4, D and F). Thus, GPNMB is necessary for the robust internalization of aSyn into iPSC-Ns.

To test whether GPNMB is also sufficient for aSyn internalization, we turned to a cell line that does not internalize aSyn at baseline. In HEK293 cells, GPNMB is expressed at very low levels endogenously and, in the absence of exogenous GPNMB expression, aSyn was not taken up by cells (Fig. 4E, top row). However, expression of GPNMB, but not of a control transmembrane protein (TMEM106B), conferred the ability to internalize aSyn (Fig. 4, E and G). Thus, GPNMB is sufficient for the internalization of aSyn.

GPNMB expression is permissive for the development of aSyn pathology in neurons

Having demonstrated that GPNMB is needed for robust internalization of fibrillar aSyn in iPSC-Ns, we next investigated whether loss of GPNMB would rescue the development of aSyn pathology in these cells. To test this, we introduced aSyn PFFs into the culture medium of GPNMB WT, Het, and KO iPSC-N lines at the same time point as the internalization experiments (day 14 after neuronal induction) and then continued to culture the neurons for 14 more days after the one-time addition of fibrillar aSyn. At the end of this period, in WT neurons, as expected, we observed abundant examples of S129-phosphorylated aSyn (Fig. 5A, second row), often along neuronal processes (Fig. 5C). In GPNMB Het or KO neurons, however, minimal phospho-aSyn staining was found (Fig. 5A). By extracting soluble proteins from our neuronal cultures, we found that WT GPNMB iPSC-Ns developed insoluble aSyn aggregates to a much greater degree than GPNMB Het or KO neurons (Fig. 5B, second row). These insoluble aggregates had a dense appearance and were often found in a perinuclear location (Fig. 5E). Moreover, quantifications of S129-phosphorylated aSyn, with (Fig. 5F) or without (Fig. 5D) first extracting soluble proteins, revealed a >70% reduction in hyperphosphorylated aSyn species in the *GPNMB* Het and KO neurons. Thus, GPNMB functions in the development of PD pathology through mechanisms related to the cellular internalization of fibrillar aSyn.

GPNMB measures reflect clinical status in PD

Findings from our human eQTL and ASE analyses and iPSC-N experiments support a model
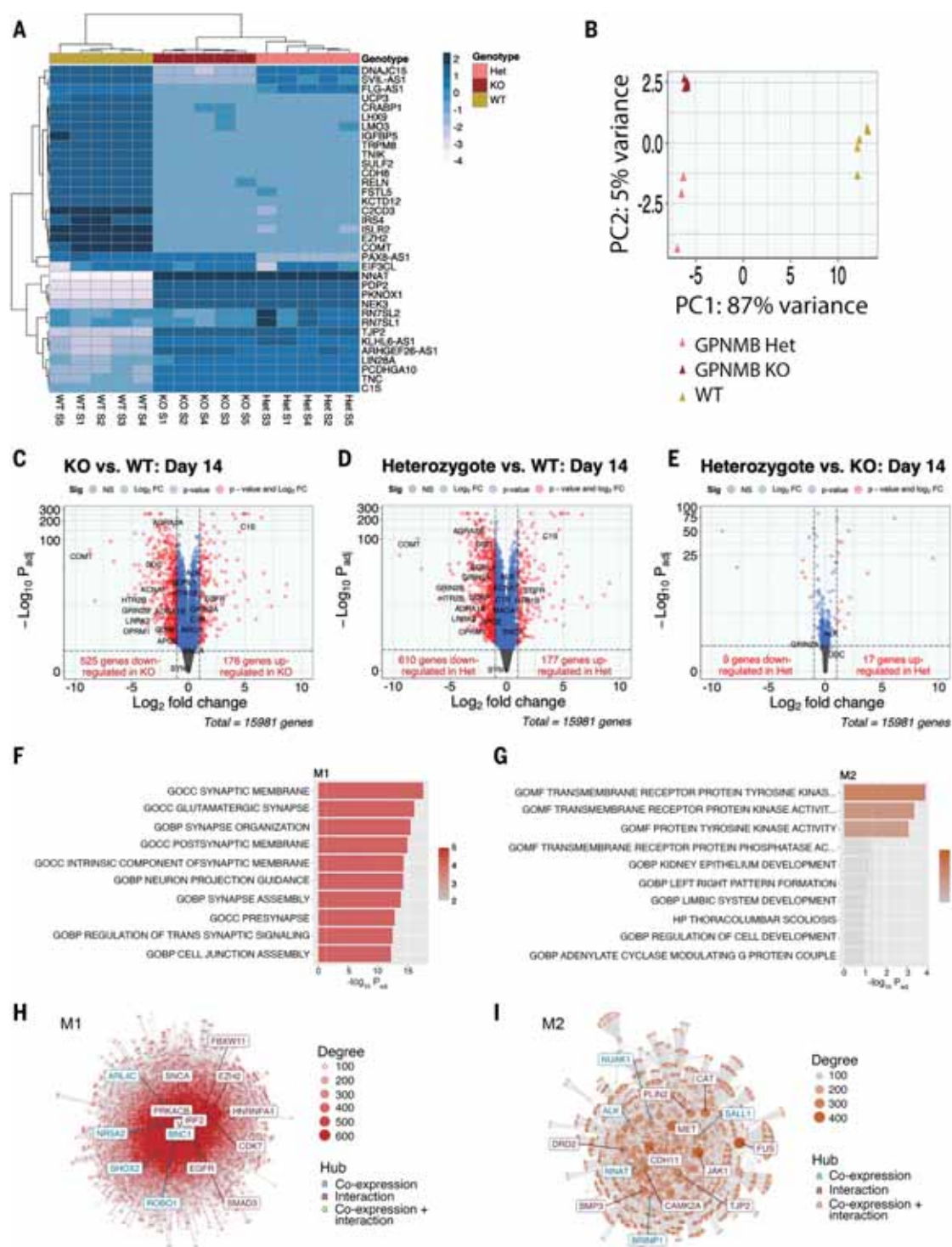
Fig. 3. Transcriptomic profiling of iPSC-Ns with heterozygous or homozygous loss of GPNMB reveals altered synaptic biology. (**A**) Heatmap showing clustering of iPSC-Ns (day 14 after neuronal induction) based on the top 35 genes. $N = 5$ replicate samples from three independent neuronal differentiations per *GPNMB* genotype. (**B**) PCA using all expressed genes. (**C** to **E**) Volcano plots for pairwise comparison of GPNMB KO cells compared with WT (C), GPNMB Het cells compared with WT (D), and GPNMB KO cells compared with Het (E). The horizontal axes indicate the log$_2$ fold-change (log$_2$FC) in gene expression. The vertical axes indicate the −log$_{10}$ of Benjamini-Hochberg–adjusted P value (P_{adj}), with dotted lines

indicating a $P_{adj} = 0.01$ significance threshold. (**F** and **G**) Two coexpression modules (M1 and M2) differentiated WT iPSC-Ns from GPNMB Het and KO iPSC-Ns. The top 10 enriched pathways for M1 (F)—decreased in GPNMB Het and KO iPSC-Ns—and M2 (G)—increased in GPNMB Het and KO iPSC-Ns—are listed. (**H** and **I**) Network analysis of genes in modules M1 (H) and M2 (I) constructed using the GeneMANIA (*25*) protein-protein interaction dataset. Each point represents a gene, with edges showing protein-protein interactions or coexpression. The most connected genes, or hubs, are labeled, with teal representing coexpression hubs and maroon representing protein-protein interaction hubs.
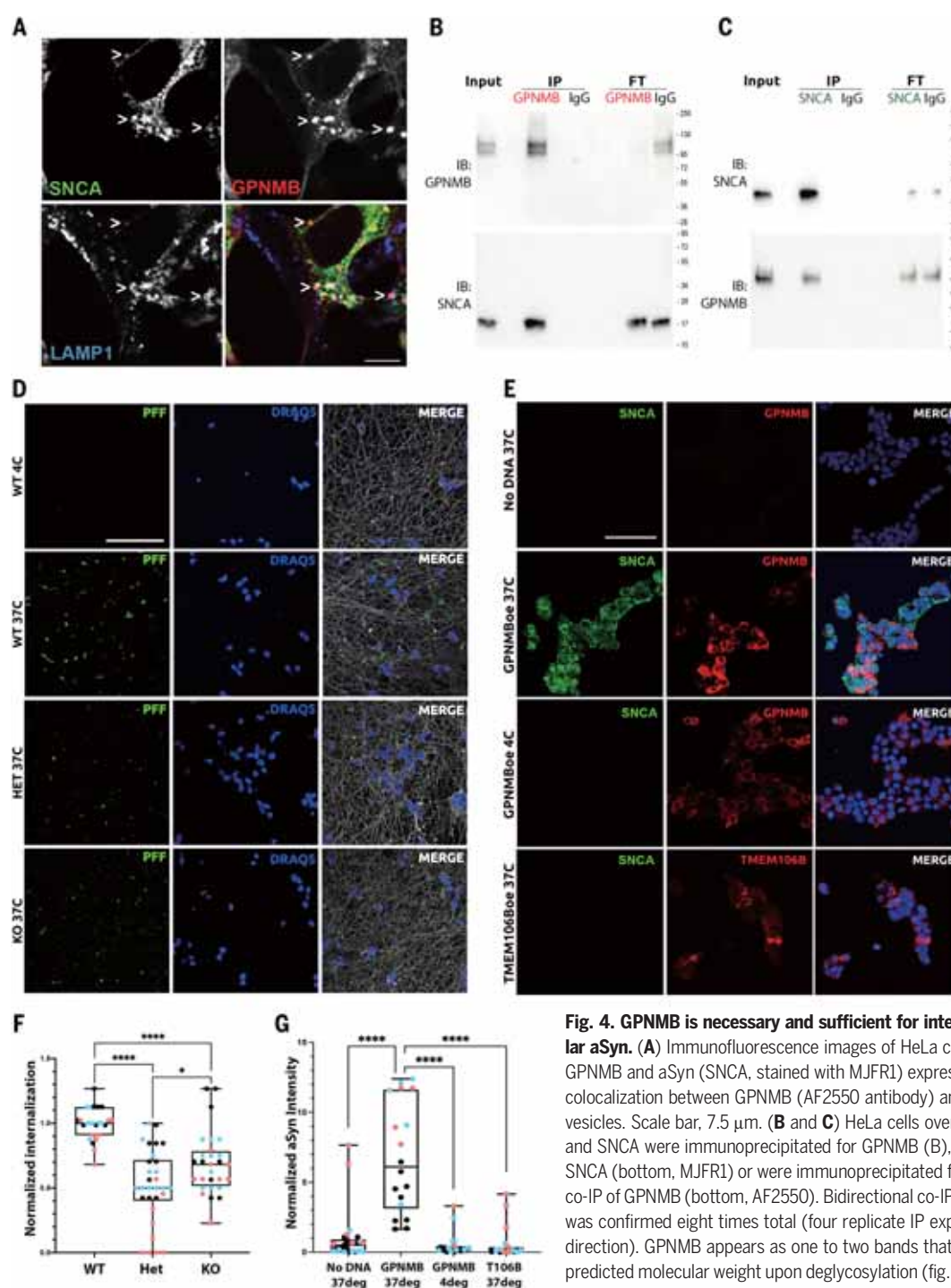
Fig. 4. GPNMB is necessary and sufficient for internalization of fibrillar aSyn. (**A**) Immunofluorescence images of HeLa cells transfected with GPNMB and aSyn (SNCA, stained with MJFR1) expression constructs show colocalization between GPNMB (AF2550 antibody) and SNCA in LAMP1+ vesicles. Scale bar, 7.5 μm. (**B** and **C**) HeLa cells overexpressing GPNMB and SNCA were immunoprecipitated for GPNMB (B), showing co-IP of SNCA (bottom, MJFR1) or were immunoprecipitated for SNCA (C), showing co-IP of GPNMB (bottom, AF2550). Bidirectional co-IP of GPNMB and SNCA was confirmed eight times total (four replicate IP experiments from each direction). GPNMB appears as one to two bands that collapse to the predicted molecular weight upon deglycosylation (fig. S2). 1:10:1 Input:IP:FT (flow-through) for protein loading on immunoblots. (**D**) Representative images of Alexa Fluor 594 (AF594)–labeled human aSyn PFFs internalized in iPSC-Ns (DIV14). All experiments were started at 4°C to allow for addition of PFF in the absence of active uptake. Cells were then maintained at 4°C (top row: negative control) or warmed to 37°C for 90 min to permit uptake (WT, GPNMB Het, and GPNMB KO are shown in rows 2, 3, and 4, respectively). Monochrome images were captured by confocal microscopy, then converted to color for visualization using FIJI software. In each case, PFFs are shown in green, nuclei are shown in blue, and β-tubulin (neuronal structural marker) is shown in gray. Scale bar, 50 μm. Only WT iPSC-Ns demonstrate definite uptake of aSyn PFF. (**E**) Representative images of HEK293 cells, a human cell line that does not internalize aSyn PFF at baseline (top row: negative control). Overexpression of GPNMB (red, stained with D9 antibody) enables internalization of human WT PFFs (SNCA, green, stained with MJFR1 antibody) at 37°C (row 2). However, no internalization is observed when GPNMB-overexpressing cells are maintained at 4°C (row 3) or at 37°C when another protein (TMEM106B) is overexpressed in HEK293 cells (row 4, TMEM106B is shown in red for this row only, FLAG tag stained). Monochrome images were captured by confocal microscopy, then processed using FIJI imaging software. Nuclei are shown in blue. Scale bar, 50 μm. (**F**) Quantification of aSyn PFF uptake in iPSC-N lines. N = 30 images from three independent differentiations (blue, pink, and black dots) per iPSC-N line. Groups were compared by Mann-Whitney test. *P < 0.05; ****P < 0.0001. (**G**) Quantification of aSyn PFF uptake in HEK293 cells. N = 30 images from three independent transfections (blue, pink, and black dots) per condition. Groups were compared by Mann-Whitney test. ****P < 0.0001. Boxplots [(F) and (G)] depict median, 25th, and 75th quartiles, and whiskers depict full ranges.
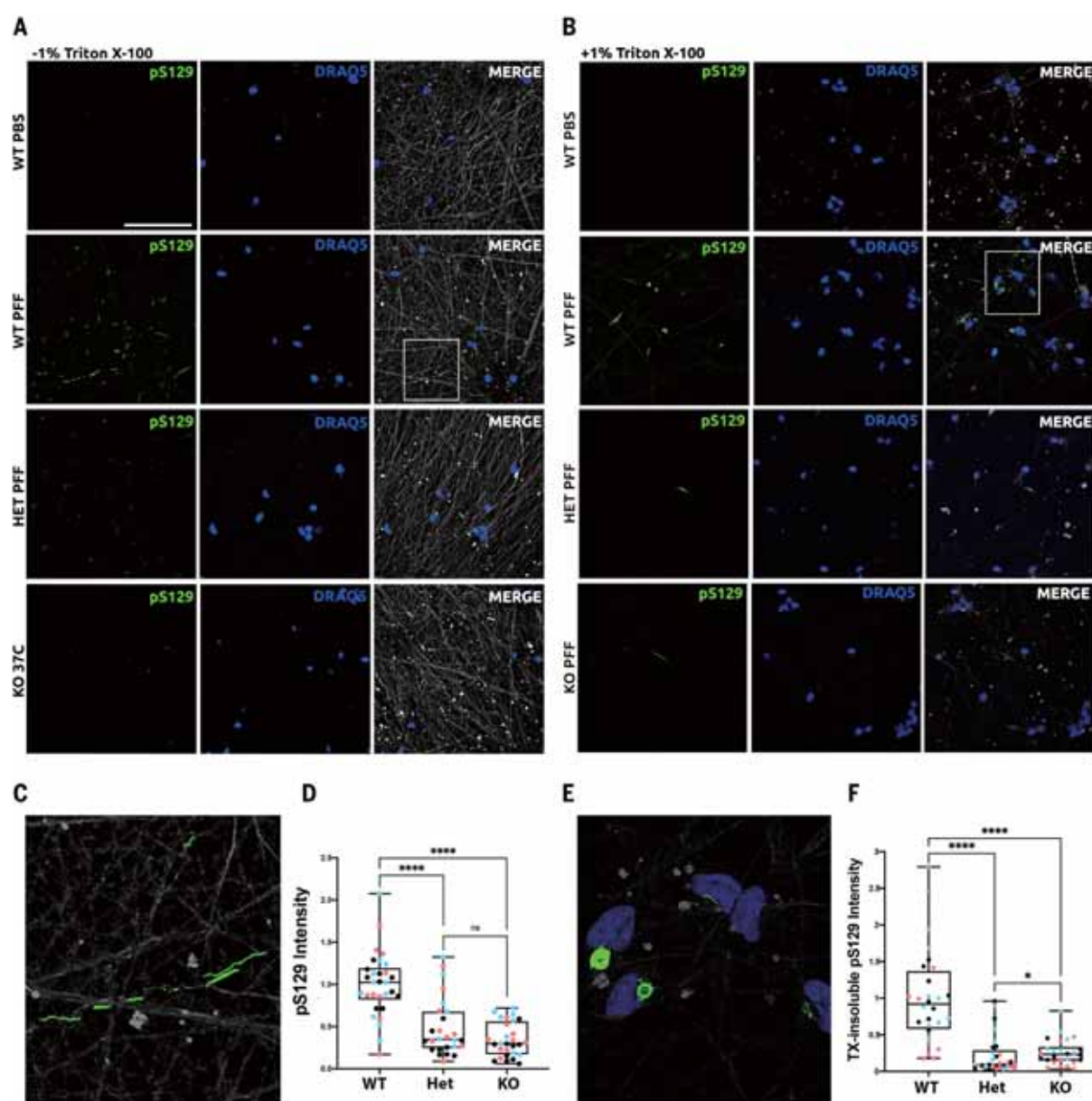
Fig. 5. GPNMB is necessary for development of aSyn pathology in iPSC-Ns.
(**A** and **B**) Untagged human aSyn PFFs were added to iPSC-Ns at DIV14. Neuronal cultures were maintained for 14 additional days to allow for development of aSyn pathology before cells were washed, fixed, and stained under conditions without 1% Triton X-100 (TX) extraction (A) or after extraction of soluble proteins with 1% TX (B). 81a antibody against aSyn phospho-S129 (pS129) was used to stain pathology (green). Neurons were also stained for nuclear DNA (blue) and tubulin (gray), although this structural protein was largely removed under 1% TX extraction conditions. Scale bar, 50 μm. For each set, a negative control condition without addition of aSyn PFFs is shown in the top row, followed by addition of aSyn PFFs in WT (row 2), GPNMB Het (row 3), and GPNMB KO (row 4) iPSC-Ns. Only the WT iPSC-Ns demonstrate abundant pS129 staining. (**C** and **E**) The pS129 staining shows a neuritic pattern [(C), inset from (A)] in the absence of 1% TX extraction and a dense perinuclear aggregate pattern [(E), inset from (B)] after extraction of soluble proteins, only in the WT iPSC-Ns. (**D** and **F**) Quantification of pS129 pathology scores is shown under conditions without 1% TX (D) and after extraction of soluble proteins with 1% TX (F). *N* = 30 images from three independent differentiations (shown as blue, pink, and black dots) per line. Boxplots depict median, 25th, and 75th quartiles, and whiskers depict full ranges. Groups were compared by Mann-Whitney test. ****P < 0.0001; *P > 0.05.

in which higher *GPNMB* expression levels confer risk for PD through interactions with aSyn that are permissive for neuronal internalization of fibrillar aSyn. Because the extracellular domain of GPNMB is known in cancer contexts to be shed and to circulate in bodily fluids, we explored whether GPNMB might be detected in plasma and cerebrospinal fluid (CSF)

samples from 731 PD and 59 NC individuals (Fig. 6; also see demographic data in tables S4 to S7). Furthermore, we sought to understand whether GPNMB measures in biofluids from living subjects might reflect either rs199347 genotype or disease.

Echoing our results from eQTL and ASE analyses in human brain samples (Fig. 1), we

found that rs199347 genotypes associated with GPNMB levels in CSF in the direction predicted by GTEx (*10*), whereas no protein quantitative trait locus (pQTL) effect was observed in the plasma (Fig. 6, A and B). Notably, however, plasma GPNMB levels were elevated in PD individuals compared with NCs (Fig. 6C), and this elevation persisted after adjustment
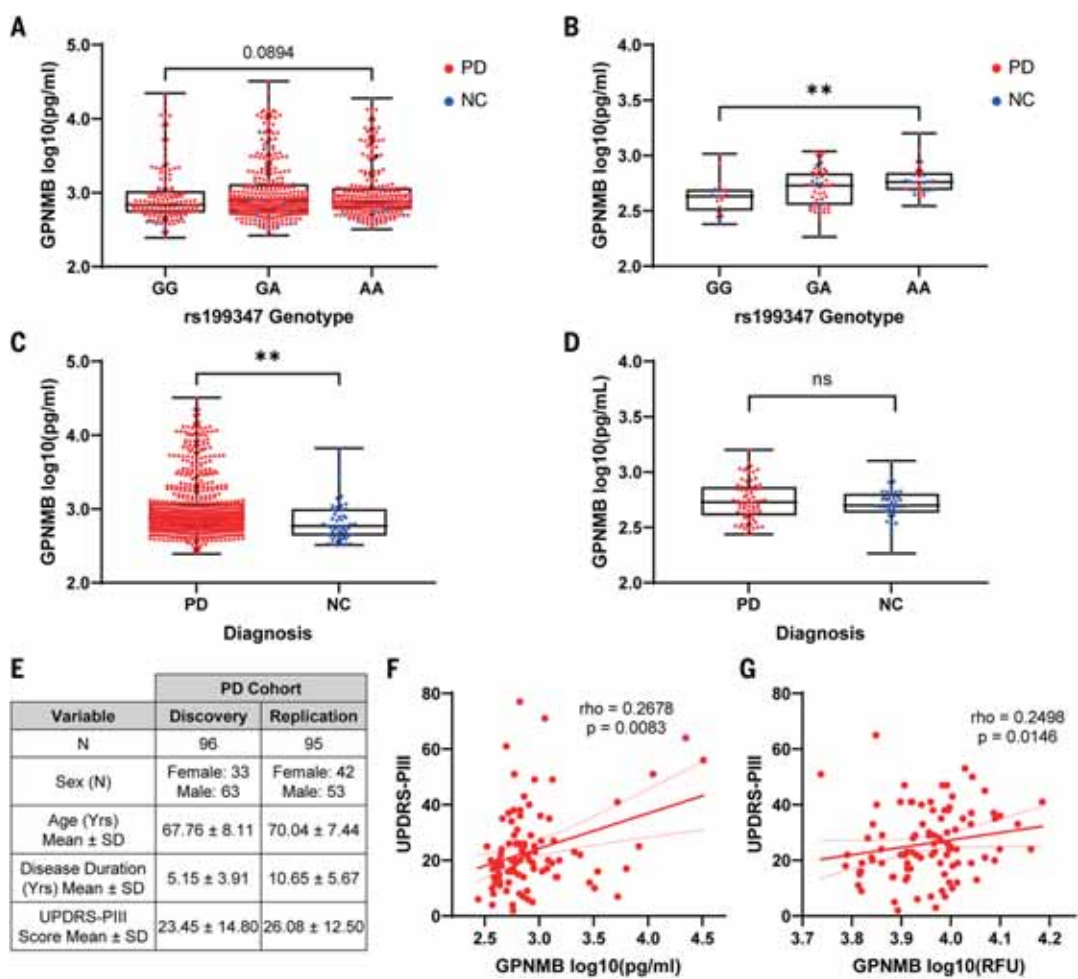
Fig. 6. Biofluid GPNMB protein levels associate with rs199347 genotype, PD diagnosis, and disease severity. (**A** and **B**) Plasma (A) and CSF (B) GPNMB levels grouped by rs199347 genotype. Genotypes were compared with Kruskal-Wallis test, followed by post hoc Dunn's test. **P < 0.01. (**C** and **D**) Plasma (C) and CSF (D) GPNMB levels grouped by diagnosis. PD (red) versus NCs (blue) were compared by Mann-Whitney test. Boxplots depict median, 25th, and 75th quartiles, and whiskers depict full ranges. **P < 0.01. (**E**) Demographics for discovery and replication cohorts used for UPDRS-PIII analysis. (**F** and **G**) Scatterplots showing positive correlation between UPDRS-PIII scores and plasma GPNMB values in discovery (F) and replication (G) cohorts. Spearman's rho and P value are displayed. RFU, relative fluorescence unit.

for age, sex, and rs199347 genotype (β_{PDvsNC} = 0.141, P = 0.0397; tables S8 and S9). Moreover, in a subset of 96 PD individuals with clinical severity measures (Fig. 6E), plasma GPNMB levels were associated with disease severity as measured by the Unified Parkinson's Disease Rating Scale Part III (UPDRS-PIII) score (*27*), with higher plasma GPNMB levels found in more severely affected PD patients (Fig. 6F and table S10).

We confirmed these results in a second cohort of PD individuals from whom we had previously obtained GPNMB plasma measures using an aptamer-based method (*28*). Despite differences in measurement platform, disease duration, and severity between the original cohort of 96 individuals and this cohort of 95 additional, nonoverlapping PD individuals, GPNMB levels replicated their association with disease severity (Fig. 6G and table S11).

Discussion

Using statistical genetic methods, direct measures of ASE in human brain samples, CRISPR-based manipulation of gene levels in iPSC-Ns, and human biomarker studies, we establish *GPNMB* as a PD risk gene. Moreover, using a PD cellular model, we nominate GPNMB as a potential therapeutic target for interrupting the transmission of pathological aSyn. Finally, we demonstrate the importance of GPNMB expression levels, with even partial loss of expression exerting profound effects on aSyn and the synapse and increased expression associating with clinical severity in PD. Our results support a model in which PD risk–associated haplotypes at the rs199347 locus result in increased expression of *GPNMB* at the RNA and protein levels. Increase in *GPNMB* expression, in turn, may confer risk for development of PD through effects on the synapse and specifically on the cellular uptake of pathological forms of aSyn.

In this work, we integrated computational analyses of large databases with direct experimental verification of key predictions from these analyses. For example, statistical colocalization techniques and eQTL analyses suggested that the rs199347 haplotype affects *GPNMB* expression levels, and direct measures of *GPNMB* ASE in human brain samples confirmed these effects. Similarly, transcriptomic profiling of GPNMB-edited iPSC-Ns revealed broad effects on the synapse, with aSyn emerging as a hub protein from network analyses of genes affected by loss of GPNMB, and our cell biological studies confirmed a functional GPNMB-aSyn interaction with repercussions for the cellular transmission of pathological aSyn.

Additionally, we integrated the use of patient-derived samples with bench-based manipulation in a model system. The failure, to date, of many cell- and mouse model–based findings to translate to clinical utility in PD underlines the

importance of verifying that biological pathways implicated in model systems show corresponding signals in human disease. We used ~800 human samples to ground our study in clinical relevance. Direct manipulation of GPNMB in iPSC-Ns then allowed us to establish a causal effect for GPNMB in cellular processes that may mediate PD pathology.

What remains to be seen is whether GPNMB interacts with both normal and pathological conformations of aSyn to a similar extent and whether our neuronal findings will translate in vivo. A detailed analysis of the interaction between these two proteins, including whether the interaction with aSyn occurs with the soluble form of GPNMB versus the transmembrane protein before cleavage, would be key to downstream attempts at targeting. However, the discovery of a protein, expressed at the cell surface, which is both necessary and sufficient for internalization of fibrillar aSyn in neurons, opens up therapeutic avenues in PD.

Materials and methods

A more detailed version of the materials and methods is provided in the supplementary materials.

RNA isolation and library preparation from human brain samples

Human postmortem brain samples from NCs (n = 2) and PD (n = 4) individuals were obtained from the University of Pennsylvania Center for Neurodegenerative Disease Research (CNDR) Brain Bank and dissected as previously described (*29*). Demographics are summarized in table S1. The regions analyzed included the caudate nucleus, cingulate gyrus, and cerebellum. Samples were made up of predominantly gray matter. Genotypes for the brain samples were obtained as previously described (*29*, *30*).

Library preparation was performed with the KAPA RNA HyperPrep Kit (KR1350, Illumina Platforms, Roche, WI). Briefly, RNA was fragmented using heat and magnesium for 8 min at 94°C to obtain 100– to 200–base pair (bp) fragments. The first cDNA strand was then synthesized using a thermocycler, followed by the second strand synthesis combined with A-tailing. Unique adapters were then ligated onto the library insert fragments and amplified using high-fidelity, low-bias polymerase chain reaction (PCR). The products then underwent a bead-based cleanup for purification of the cDNA libraries.

SeqCap RNA Choice™ probe pool design

The SeqCap RNA probe design pool was designed by Roche Sequencing Solutions Custom Design (Roche, WI). The pool was designed to contain probes ~60 bp in length with no more than 20 close matches in the genome, as determined by the Sequence Search and Align-ment by Hashing Algorithm (SSAHA), for the purposes of providing sufficient coverage of transcripts of interest while minimizing potential off-target effects. A close match was defined as any genomic sequence that differed from one of the probe sequences by five or fewer single-base insertions, deletions, or substitutions. The majority of included probes had no off-target matches, with an exceedingly small percentage of probes displaying very few off-target matches. Only exonic probes covering the transcripts of interest were included and, to minimize SNP-mediated capture bias, probes that overlapped any SNPs in linkage disequilibrium ($r^2 > 0.2$, where r^2 is the coefficient of determination) with the sentinel PD GWAS SNPs were excluded.

Target cDNA enrichment and sequencing

Target cDNA enrichment and sequencing was performed as previously described (*14*) using the SeqCap EZ Accessory kit v2 (07145594001, Roche, WI). Briefly, equimolar amounts of cDNA libraries were combined for a total mass of 1 μg. Each of these libraries underwent multiplexed PCR with unique index oligonucleotides. The libraries were then hybridized with capture probes using the SeqCap EZ Hybridization and Wash Kit (05634261001, Roche, WI). Libraries were dried with heat in a vacuum and resuspended with hybridization reagents. Pooled capture probes for each region were added to the resuspended libraries and incubated for 20 hours in a thermocycler at 47°C, with the lid temperature at 57°C. The captured multiplex cDNA samples then underwent stringent washing steps and were amplified using ligation-mediated PCR (LM-PCR). These post-capture PCR-amplified libraries were pooled and sequenced on two lanes of an Illumina HiSeq 2500 with 150-bp paired-end reads, yielding ~150 million read pairs per lane.

Read mapping and ASE analyses

To assess RNA-seq reads quality, we used FastQC (*31*), and for reads quality filtering and trimming we used Trimmomatic (version 032) (*32*). We ran Trimmomatic to remove low-quality fragments in a 4-base-wide sliding window (average window quality below PHRED 20), and low-quality leading and trailing bases (below PHRED 10). We also dropped all the reads with average PHRED quality below 25, as well as reads shorter than 75 bases. Depending on the sample, 65 to 80% of reads passed this trimming and filtering step, resulting in 6.5 to 24 million read pairs per sample for mapping.

To perform unbiased allele-specific read mapping to the reference human genome (hg19) we applied WASP–STAR pipeline (fig. S7). First, we mapped reads with STAR (*33*), applying 2-step alignment and filtering them for mapping bias using WASP (*34*). Before proceeding with variant calling, we removed duplicate reads using rmdup_pe.py script incorporated into WASP pipeline. To call and filter single-nucleotide variants (SNVs), we used GATK tools: HaplotypeCaller, SelectVariants, and VariantFiltration. We obtained allele-specific read counts by GATK – ASEReadCounter. To filter out intergenic variants, we functionally annotated SNVs using VariantAnnotation (*35*) and TxDb.Hsapiens.UCSC.hg19.knownGene (*36*) R packages. To test for ASE at the gene level, we first selected proxy SNPs that were highly linked ($r^2 > 0.6$) with rs199347 and located within a coding region for the gene of interest to assign allele of origin. For *GPNMB*, we assigned the allele of origin for each transcript read based on genotype at rs199355, and for *KLHL7*, we assigned the allele of origin based on genotype at rs2072368. We then tested for allelic imbalance with a beta-binomial model with overdispersion using the MBASED R package (*13*). *P* values were adjusted for false discovery rate using the Benjamini-Hochberg method (*37*).

Colocalization analysis

Colocalization analysis was performed as previously described (*11*) using the coloc package in R (version 4.0-2). The prior probabilities of p1, p2, and p12 were set to 1×10^{-4}, 1×10^{-4}, and 1×10^{-5} respectively. Significant colocalization was determined as having a PPH4 > 75%. Sensitivity analysis was performed to determine whether PPH4 is robust over plausible values of p12 (1×10^{-5} to 1×10^{-6}) (*38*). Association plots were generated using Locus-Comparer package (version 1.0.0) (*39*) in R.

Immortalized cell line transfection and collection

For co-IP experiments, HEK293 or HeLa cells were plated at 700,000 or 1 million cells per well, respectively, and 18 hours after plating, transfection was performed with 4 μg of each DNA construct and Lipofectamine 2000 (Thermo Scientific) in serum-free Dulbecco's minimum essential medium (DMEM). Cells were transfected with either GPNMB-myc-DDK pCMV6-Entry (Origene) and 5′ untranslated region (5′ UTR)–Syn pcDNA3.1+ (obtained from K. Luk) for the GPNMB-flag IP or GPNMB untagged clone pCMV6-XL4 (Origene) and Syn-Myc pcDNA3.1+ (obtained from K. Luk) for the Syn-Myc IP. Four hours after transfection, media was changed to DMEM with 10% fetal bovine serum (FBS), 1% L-Glut, and 1% Pen-Strep. At 20 hours posttransfection, cells were washed in Dulbecco's phosphate-buffered saline (dPBS) and lysed in CHAPS buffer (25 mM Tris, 150 mM NaCl, 1 mM EDTA, 1% CHAPS, 5% glycerol, pH to 7.4). Lysates were collected and spun down at 4°C for 30 min at 21380 xg. Bicinchoninic acid (BCA) assays (Thermo Scientific) were used to determine protein concentrations.

For immunofluorescence experiments, HEK293 or HeLa cells were plated at either 100,000 or

200,000 cells per well on either PDL-coated or untreated 12-mm glass coverslips in a 12-well format. 18 hours after plating, the cells were transfected with 1.6 μg of each DNA construct (GPNMB untagged clone pCMV6-XL4 and 5′ UTR-Syn pcDNA3.1+) and Lipofectamine 2000 (Thermo Scientific) in serum-free DMEM.

Co-IP

To immunoprecipitate GPNMB, 300 μL of anti-Flag–conjugated beads (Sigma A2220) or mouse immunoglobulin G (IgG)–conjugated beads (Sigma A0919, used as a negative control) were used to immunoprecipitate from 1000 μg of lysate from GPNMB-myc-DKK and 5′UTR-syn double-transfected cells in CHAPS buffer overnight at 4°C. To immunoprecipitate aSyn, 300 μL of anti-c-Myc-conjugated beads (Sigma A7470) or rabbit IgG-conjugated beads (Sigma A2909, used as a negative control) were used to immunoprecipitate from 1000 μg of lysate from GPNMB untagged clone and Syn-Myc double-transfected cells in CHAPS buffer overnight at 4°C. After 24 hours, the protein-conjugated beads were washed three times with CHAPS buffer and the bound protein was competitively eluted from the beads using either 250 μM 3x flag peptide (Sigma) or 250 mM myc peptide (Sigma) for 1 hour at 4°C.

CRISPR-Cas9 KO of human iPSCs

Human iPSCs with *Neurog1* and *Neurog2* in a bicistronic doxycycline-inducible expression cassette (*22*) were used for generation of *GPNMB* KO iPSCs and rapid induction of iPSC-Ns. The protocol for generating CRISPR-edited iPSCs is summarized in fig. S3 and detailed in the supplementary materials and methods.

Culture and differentiation of iPSC-Ns

Before differentiation, iPSC cultures were maintained on Matrigel-coated 6-cm tissue culture plates with mTeSR1 media and mechanically passaged every 4 days with StemMACS passaging solution XF. The neural induction protocol is summarized in fig. S4, based on prior studies (*40*), and detailed in the supplementary materials and methods.

Immunofluorescence

The media was aspirated from coverslip-containing wells, and the cells were fixed in 2% paraformaldehyde in dPBS for 15 min at room temperature. After fixing, the coverslips were rinsed five times with dPBS and blocked/permeabilized with blocking buffer (3% bovine serum albumin + 0.05% saponin in dPBS) for 1 hour before incubating in primary antibody overnight. Image stacks of 1-μm thickness were acquired by confocal microscopy (Leica SP5) using a 40x oil immersion objective with 2x zoom. Antibody concentrations are summarized in the key resources tables in the supplementary materials.

Image processing and quantification

Image processing to quantify synaptic proteins was performed using a Cell Profiler pipeline based on Danielson *et al.*'s previously published work (*41*). A single slice was chosen from each stack to focus our analysis on the plane with the most abundant synapsin-1 staining. TUBB3 images underwent image enhancement for neurite-like features and were used to calculate TUBB3+ area for normalization and expanded to generate a mask. Synapsin-1 and aSyn images underwent enhancement for speckle-like features, followed by object identification and characterization of object size/intensity. The total integrated intensity (i.e., sum for all particles) was used for analysis. The pipeline used has been made publicly available in the supplementary materials.

aSyn pathology in iPSC-Ns was also quantified using CellProfiler. Maximum intensity projections of z-stack images were created using FIJI. Desired 81a+ objects were identified with intensity thresholding and the total area of 81a+ objects were normalized with total area of DRAQ5+ objects. To quantify MJFR1+ staining in HEK293 overexpressing GPNMB, nuclei artifact staining was removed by generating DRAQ5+ nuclei mask and excluding MJFR1+ speckles within the mask. Total area of MJFR1+ objects was normalized by total area of DRAQ5+ objects.

A researcher blinded to sample identity was provided with randomly ordered maximum intensity projection of z-stack images of iPSC-Ns treated with AF594-PFF. Scores ranging from 0 to 3 were given for each criterion: intensity, length, and frequency of internalized PFFs. The three scores were added and were normalized to the average score of WT iPSC-Ns.

Synaptosome extraction

Synaptosomes were extracted using Syn-PER Synaptic Protein Extraction Reagent (Thermo-Fisher) per the user instructions.

Immunoblotting

Samples were diluted in 5X concentrated sample buffer [10 g Sucrose, 1.85 mL 0.5 M Tris, pH 6.8, 1.0 mL 0.1 M EDTA, 1.0 mL of 0.1% Bromophenol Blue, 1.0 mL of 0.05% Pyronine Yellow, 0.615 g of dithiothreitol (DTT), 10 mL of 10% sodium dodecyl sulfate (SDS), and adjusted to a final volume of 20 mL with Milli-Q Water] and boiled at either 100°C for 10 min or 70°C for 15 min for heat-sensitive proteins (GPNMB). Samples were run on 4 to 20% polyacrylamide TGX gels (Bio-Rad Laboratories) and transferred onto 0.2 nitrocellulose membrane (Bio-Rad Laboratories). When blotting for aSyn, membranes were fixed in 0.4% PFA for 30 min (*42*). Membranes were blocked in 5% milk in tris-buffered saline (TBS) for 1 hour and blotted overnight at 4°C with specific antibodies. The membranes were incubated for 2 hours in horseradish peroxidase (HRP)–conjugated secondary antibodies and developed using Western Bright ECL and Sirius HRP substrates (Advansta). Antibody concentrations are summarized in the key resources tables. Densitometry was performed using the Bio-Rad Image Lab Software.

RNA-seq of iPSC-Ns

RNA was extracted from iPSC-Ns on days 0 and 14 after doxycycline induction using QIAGEN RNAeasy mini kit. RNA integrity was measured using RNA nano chips (Agilent) on an Agilent 2100 Bioanalyzer. All samples had RIN > 9.4. Library preparation was performed with the TruSeq Stranded mRNA Library Prep kit (Illumina cat no. 20020595) using 225 ng of total RNA and following manufacturer instructions. High-sensitivity DNA chips (Agilent) were used to balance libraries before sequencing. In total, 30 RNA samples [three genotypes (WT, Het, and KO) × two differentiation times (days 0 and 14) × five biological replicates] were sequenced. All 30 samples were sequenced together on a single S2 flow-cell generating >1.1×10^9 of 100-bp single-end reads in total (on average 3.69×10^7 reads per sample, ranging from 2.9×10^7 to 5.3×10^7). A summary of the Illumina NovaSeq run is provided in table S12.

Read quality control and filtering

A quality check of the raw reads was assessed using FastQC (*31*) and summarized with MultiQC (*43*). Next, the adapters were removed and filtering of the low-quality reads was conducted using Trimmomatic, version 0.39 (*32*), with the following parameters: *ILLUMINACLIP: TruSeq3-SE.fa:2:30:10 LEADING:5 TRAILING:5 SLIDINGWINDOW:5:20 MINLEN:50 AVGQUAL:30 HEADCROP:10*. The adapters that matched the sequences provided by TruSeq3-SE.fa were removed. The low-quality bases were cut off the start and off the end of reads if their PHRED score was below 5. The sliding window of 5 bp was applied to trim the bases if the window PHRED score dropped below 20. The 10 bases from the start of the reads were also cropped. Finally, the reads were discarded if the average PHRED score of the read was below 30.

Read alignment and quantification

The sequence alignment BAM files generated by Bowtie 2 were used as the input to RSEM software tool, to quantify gene expression levels (*44*). On average, 3.61×10^7 (97.8%) of reads per sample passed the filtering steps and were mapped versus reference genome GRCh38 using Bowtie 2 with the following parameters: *bowtie2 -q–phred33–sensitive–dpad 0–gbar 99999999–mp 1,1–np 1–score-min L,0,-0.1–nofw -p 32 -k 200 -x*, as suggested by RSEM manual. The read alignment rate was on average >89% (table S12). To obtain the raw read counts at the gene level, an expectation

maximization algorithm (RNA-seq by Expectation Maximization) was run by the following RSEM command: *rsem-calculate-expression–bowtite2–forwardprob 0*.

Differential gene expression (DGE) analysis

To detect significant differences in iPSC-N gene expression data between day 0 and day 14 and between the genotypes (WT, Het, and KO), DESeq function form DESeq2 Bioconductor's R package (*45*) was used. RNA-seq data were modeled using the negative binomial distribution that accounts for overdispersion. To conduct the pairwise comparisons (day 14 versus day 0 in WT, KO versus WT, Het versus WT, and KO versus Het at day 14) for each gene, the *nbinomWaldTest* statistic was used. The Wald test P values were calculated by scaling the coefficients by their standard errors and then compared with a standard Normal distribution. After DGE analysis, the lfcShrink function from R package apeglm (*46*) was applied to shrink the log2FC. We corrected for false discovery rate (FDR) using the Benjamini-Hochberg method (*37*). Genes with a Benjamini-Hochberg–corrected $P < 0.01$ and a |log2 fold-change| > 1 were considered to be significantly differentially expressed. To visualize the results of DGE analyses we used EnhancedVolcano R package version 1.10.0 (*47*).

Modular coexpression network analysis

Modular coexpression network analysis of iPSC-Ns was performed using R package *CEMiTool* (CoExpression Molecules identification Tool), version 1.14.1 (*48*). The rlog normalized expression data (15981 genes in 15 samples) were used as an input to *cemitool* function. As a first step, cemitool conducted an unsupervised filtering of expression data using the inverse gamma distribution to model the variance of genes. Out of 15981 genes, 1100 genes with $P < 0.1$ survived this filtering and were used for downstream analyses. The genes were then separated into modules using the dissimilarities measures and the *Dynamic Tree Cut* package (*49*). The minimum number of genes per module was set to 20, and similar modules were merged together based on correlation.

To determine biological functions associated with the coexpression modules, the gene ontology (GO) gene sets *c5.all.v7.4*, which contain GO resources (BP, biological process; CC, cellular component; MF, molecular function) and human phenotype ontology (HPO) from MSigDB database (*50*), were used in overrepresentation analysis (ORA). The module gene set enrichment analysis (GSEA) was performed using the *fgsea* R package (*51*) within the CEMitool pipeline. First, a z-score gene normalization on all input genes was performed, followed by calculation of the mean for each sample class (GPNMB WT, Het, and KO). Next, a preranked GSEA was performed

independently for each *GPNMB* genotype. The module activity was visualized by normalized enrichment score.

To construct the gene interactions network in the coexpression modules, the combined human protein-protein interaction data, downloaded from GeneMANIA, were added to the CEMiTool object using the function *interactions_data*. The interactions between the genes were visualized using the *plot_interactions* function.

aSyn PFF internalization and immunofluorescence experiments

Human WT PFFs and fluorescent fibrils including Alexa Fluor594 (AF594)–conjugated aSyn were provided by K. Luk at the Penn CNDR. All fibrils were kept at –80°C until use. After the stock of 5 mg/mL was diluted to a working concentration of 0.1 mg/mL in dPBS, fibrils were sonicated (Diagenode Biorupter Plus) on high, sonicating for 30 s followed by 30 s of rest for a total of 10 min. Sonicated PFFs were then added to classic neuronal media according to appropriate concentrations.

For AF594-PFF internalization experiments using iPSC-Ns, 10 μg of PFFs were added per well of a 12-well plate. iPSC-Ns were incubated in 4°C for 30 min, followed by an additional 30-min incubation at 4°C for the negative control or 1 hour and 30 min in 37°C for experimental wells. All cells were immediately fixed and stained afterward.

To demonstrate aSyn pathology after PFF transduction, we replaced regular media of iPSC-Ns at day 14 with classical neuronal media containing total of 1 μg of human WT PFFs per well. iPSC-Ns were fixed and stained after 14 days (at day 28 of neuronal induction). To extract soluble proteins, coverslips were fixed with 2% paraformaldehyde and 1% Triton X-100 in dPBS. 3% bovine serum albumin without saponin in dPBS was used as blocking buffer.

For WT PFF internalization experiments using HEK293, cells were plated at 200,000 cells per well in PDL-coated 12-mm glass coverslips in a 12-well format. 18 hours after plating, the cells were transfected with 1 μg of DNA (GPNMB untagged clone pCMV6-XL4 or TMEM106B-Flag) and Lipofectamine 2000 (Thermo Scientific) in serum-free DMEM. At 20 hours posttransfection, media was replaced with DMEM containing 1 μg of PFFs per well. The plates were incubated for 30 min at 4°C followed by an additional 30-min incubation at 4°C for negative control (to inhibit endocytosis) or 1 hour and 30 min in 37°C for experimental wells. All cells were immediately fixed and stained for immunofluorescence afterward.

Patient samples and genotypes

Plasma and CSF samples of PD patients and NCs were obtained as part of the Penn CNDR Neuropathology, Biomarker, and Genetics Biobank and the Parkinson's Disease Molecular

Integration in Neurological Diagnosis Initiative (MIND) studies. PD patients had a clinical diagnosis of PD made by a movement disorders specialist at the Parkinson's Disease and Movement Disorder Clinic (PDMDC) at the University of Pennsylvania, whereas controls had no known neurological disorder. Data were stored in the Penn Integrated Neurodegenerative Disease Database (INDD) (*30*). These studies were approved by the UPenn Institutional Review Board (IORG0000029). Informed consent was obtained at study enrollment. Participant demographics are reported in tables S4 to S7. Individuals with known *GBA1* mutations (N370S, E365K, and L444P) were excluded from the analysis because GPNMB elevation has been reported in patients with Gaucher disease, a lysosomal storage disorder caused by homozygous mutations in GBA1 (*52*, *53*). Genotyping of SNP rs199347 was performed by Infinium Global Screening Assay (Illumina), NeuroX genotyping platform, PANDoRA (Sequenom) panel (*30*), or MIND panel based on allele-specific PCR performed using FlexSix Dynamic Array integrated fluidic circuits (Fluidigm) and genotyping using BioMark HD system (Fluidigm) (*54*).

A subset of PD individuals from the previously described University of Pennsylvania U19 Cohort (*55*) had UPDRS-PIII scores for disease severity.

Enzyme-linked immunosorbent assay (ELISA)

GPNMB protein levels within human plasma and CSF samples were measured with ELISA kits (R&D systems) according to manufacturer's instructions. CSF and plasma samples were diluted by factors of 1 in 2 and 1 in 30 respectively to obtain optical density measurements within the standard range. All samples were run in duplicates and absorbance at 450 nm was determined by a microplate reader (Berthold Technologies, Tristar LB 941). Only duplicate samples with a coefficient of variation (CV) of <25% were retained for analysis, and the average CV across all samples used was 3.3%. Moreover, replicate samples assayed by ELISA on different days, by different operators, across multiple freeze-thaw cycles, demonstrated excellent reproducibility (Pearson's correlation coefficient $r = 0.97$).

Multiple linear regression analyses

Multiple linear regression was used to determine factors that are significant predictors of GPNMB concentration in plasma and CSF. Age, sex, PD status, and rs199347 genotype were included as independent variables. A codominant genetic model, which considers each allele combination (GG, AG, and AA) as a separate factor (*56*), was used to model the effect of rs199347. Regression coefficients were calculated with GG as the reference.

The relationship between GPNMB levels and disease severity was established in two

different PD cohorts. GPNMB values for the discovery cohort were generated by ELISA (R&D systems), whereas GPNMB values for the replication cohort were generated using an aptamer-based platform (*26*). UPDRS-PIII values were downloaded from the Penn INDD.

Statistical analyses

Statistical analyses were performed with either PRISM or R. Data were tested for normality with a Shapiro-Walk test. Data with more than two categorical groups were analyzed by either one-way analysis of variance (ANOVA) (followed by post hoc Tukey or Dunnett tests) or Kruskal-Wallis test (followed by post hoc Dunn's test) depending on the data's distribution. Data with only two groups were analyzed by either a Welch's two-sample t test or Mann-Whitney U test depending on the data distribution. Correlations were determined using Spearman's rank correlation. Multiple linear regression (glm) was used to determine associations between two variables adjusting for potentially confounding covariates. Outlier determination was performed using ROUT method, Q (FDR) = 1%.

Immunohistochemistry

Formalin-fixed, paraffin-embedded cingulate and temporal cortex samples were obtained from the Penn CNDR. Patient demographics are reported in table S1. 6-μm sections were cleared in xylenes and a descending EtOH series. Endogenous peroxidases were quenched in 30% H_2O_2 and 70% MeOH solution for 30 min. Slides were microwaved in citric acid Antigen Unmasking Solution (Vector Laboratories). After cooling, slides were rinsed in TBS-T (0.1 M Tris Buffer/0.05% TWEEN) and blocked (TBS-T/ 2%FBS/3%BSA). Sections were incubated overnight at 4°C in the primary antibody (see the key resources tables for antibody conditions). Once washed with TBS-T, sections were incubated for 1 hour at room temperature in the secondary antibody (see the key resources tables for antibody conditions). VECTASTAIN ABC Standard (Vector Laboratories) was applied for 1 hour at room temperature followed by ImmPACT DAB (Vector Laboratories). Sections were counterstained with Harris Hematoxylin (Thermo Scientific) for 40 s. Slides were dehydrated in an ascending EtOH series and xylenes then coverslipped with Cytoseal (Thermo Scientific).

Dephosphorylation and deglycosylation

For deglycosylation of cell and brain lysates, 5.0 μL of PNGase F was added to 125 μg of brain lysates or 60 μg of cell lysates and incubated at 37°C for 30 min. For dephosphorylation experiments, 1 μL of Lambda protein phosphatase was added to 125 μg of brain lysates or 50 μg of cell lysates and incubated at 30°C for 30 min.

REFERENCES AND NOTES

1. E. R. Dorsey *et al.*, Projected number of people with Parkinson disease in the most populous nations, 2005 through 2030. *Neurology* **68**, 384–386 (2007). doi: 10.1212/01. wnl.0000247740.47667.03; pmid: 17082464

2. M. A. Nalls *et al.*, Identification of novel risk loci, causal insights, and heritable risk for Parkinson's disease: A meta-analysis of genome-wide association studies. *Lancet Neurol.* **18**, 1091–1102 (2019). doi: 10.1016/S1474-4422(19)30320-5; pmid: 31701892

3. K. McFarthing, T. Simuni, Clinical Trial Highlights: Targeting Alpha-Synuclein. *J. Parkinsons Dis.* **9**, 5–16 (2019). doi: 10.3233/JPD-189004; pmid: 30741694

4. S. A. Schneider, R. N. Alcalay, Precision medicine in Parkinson's disease: Emerging treatments for genetic Parkinson's disease. *J. Neurol.* **267**, 860–869 (2020). doi: 10.1007/s00415-020-09705-7; pmid: 31974807

5. D. Chang *et al.*, A meta-analysis of genome-wide association studies identifies 17 new Parkinson's disease risk loci. *Nat. Genet.* **49**, 1511–1516 (2017). doi: 10.1038/ng.3955; pmid: 28892059

6. M. D. Gallagher *et al.*, A Dementia-Associated Risk Variant near *TMEM106B* Alters Chromatin Architecture and Gene Expression. *Am. J. Hum. Genet.* **101**, 643–663 (2017). doi: 10.1016/j.ajhg.2017.09.004; pmid: 29056226

7. K. Musunuru *et al.*, From noncoding variant to phenotype via *SORT1* at the 1p13 cholesterol locus. *Nature* **466**, 714–719 (2010). doi: 10.1038/nature09266; pmid: 20686566

8. M. Claussnitzer *et al.*, FTO Obesity Variant Circuitry and Adipocyte Browning in Humans. *N. Engl. J. Med.* **373**, 895–907 (2015). doi: 10.1056/NEJMoa1502214; pmid: 26287746

9. F. Soldner *et al.*, Parkinson-associated risk variant in distal enhancer of α-synuclein modulates target gene expression. *Nature* **533**, 95–99 (2016). doi: 10.1038/nature17939; pmid: 27096366

10. GTEx Consortium, Genetic effects on gene expression across human tissues. *Nature* **550**, 204–213 (2017). doi: 10.1038/nature24277; pmid: 29022597

11. C. Giambartolomei *et al.*, Bayesian Test for Colocalisation between Pairs of Genetic Association Studies Using Summary Statistics. *PLOS Genet.* **10**, e1004383 (2014). doi: 10.1371/journal.pgen.1004383; pmid: 24830394

12. M. N. Murthy *et al.*, Increased brain expression of *GPNMB* is associated with genome wide significant risk for Parkinson's disease on chromosome 7p15.3. *Neurogenetics* **18**, 121–133 (2017). doi: 10.1007/s10048-017-0514-8; pmid: 28391543

13. O. Mayba *et al.*, MBASED: Allele-specific expression detection in cancer tissues and cell lines. *Genome Biol.* **15**, 405 (2014). doi: 10.1186/s13059-014-0405-3; pmid: 25315065

14. T. R. Mercer *et al.*, Targeted sequencing for gene discovery and quantification using RNA CaptureSeq. *Nat. Protoc.* **9**, 989–1009 (2014). doi: 10.1038/nprot.2014.058; pmid: 24705597

15. H. Tanaka *et al.*, The potential of GPNMB as novel neuroprotective factor in amyotrophic lateral sclerosis. *Sci. Rep.* **2**, 573 (2012). doi: 10.1038/srep00573; pmid: 22891158

16. Y. Nagahara *et al.*, GPNMB ameliorates mutant TDP-43-induced motor neuron cell death. *J. Neurosci. Res.* **95**, 1647–1665 (2017). doi: 10.1002/jnr.23999; pmid: 27935101

17. M. A. J. Weterman *et al.*, *nmb*, a novel gene, is expressed in low-metastatic human melanoma cell lines and xenografts. *Int. J. Cancer* **60**, 73–81 (1995). doi: 10.1002/ijc.2910600111; pmid: 7814155

18. A. A. N. Rose, M. Biondini, R. Curiel, P. M. Siegel, Targeting GPNMB with glembatumumab vedotin: Current developments and future opportunities for the treatment of cancer. *Pharmacol. Ther.* **179**, 127–141 (2017). doi: 10.1016/j.pharmthera.2017.05.010; pmid: 28546082

19. M. Hüttenrauch *et al.*, Glycoprotein NMB: A novel Alzheimer's disease associated marker expressed in a subset of activated microglia. *Acta Neuropathol. Commun.* **6**, 108 (2018). doi: 10.1186/s40478-018-0612-3; pmid: 30340518

20. E. B. Moloney, A. Moskites, E. J. Ferrari, O. Isacson, P. J. Hallett, The glycoprotein GPNMB is selectively elevated in the substantia nigra of Parkinson's disease patients and increases after lysosomal stress. *Neurobiol. Dis.* **120**, 1–11 (2018). doi: 10.1016/j.nbd.2018.08.013; pmid: 30149180

21. M. L. Neal, A. M. Boyle, K. M. Budge, F. F. Safadi, J. R. Richardson, The glycoprotein GPNMB attenuates astrocyte inflammatory responses through the CD44 receptor. *J. Neuroinflammation* **15**, 73 (2018). doi: 10.1186/s12974-018-1100-1; pmid: 29519253

22. V. Busskamp *et al.*, Rapid neurogenesis through transcriptional activation in human stem cells. *Mol. Syst. Biol.* **10**, 760 (2014). doi: 10.15252/msb.20145508; pmid: 25403753

23. J. E. Galvin, T. M. Schuck, V. M. Y. Lee, J. Q. Trojanowski, Differential expression and distribution of α-, β-, and γ-synuclein in the developing human substantia nigra. *Exp. Neurol.* **168**, 347–355 (2001). doi: 10.1006/exnr.2000.7615; pmid: 11259122

24. D. D. Murphy, S. M. Rueter, J. Q. Trojanowski, V. M.-Y. Lee, Synucleins are developmentally expressed, and α-synuclein regulates the size of the presynaptic vesicular pool in primary hippocampal neurons. *J. Neurosci.* **20**, 3214–3220 (2000). doi: 10.1523/JNEUROSCI.20-09-03214.2000; pmid: 10777786

25. D. Warde-Farley *et al.*, The GeneMANIA prediction server: Biological network integration for gene prioritization and predicting gene function. *Nucleic Acids Res.* **38**, W214–W220 (2010). doi: 10.1093/nar/gkq537; pmid: 20576703

26. L. A. Volpicelli-Daley, K. C. Luk, V. M.-Y. Lee, Addition of exogenous α-synuclein preformed fibrils to primary neuronal cultures to seed recruitment of endogenous α-synuclein to Lewy body and Lewy neurite-like aggregates. *Nat. Protoc.* **9**, 2135–2146 (2014). doi: 10.1038/nprot.2014.143; pmid: 25122523

27. S. Fahn, R. Elton, Members of the UPDRS Development Committee, in *Recent Developments in Parkinson's Disease*, S. Fahn, C. D. Marsden, M. Goldstein, D. B. Calne, Eds. (Macmillan Healthcare Information, 1987), pp. 153–163.

28. M. Posavi *et al.*, Characterization of Parkinson's disease using blood-based biomarkers: A multicohort proteomic analysis. *PLOS Med.* **16**, e1002931 (2019). doi: 10.1371/journal.pmed.1002931; pmid: 31603904

29. A. S. Chen-Plotkin *et al.*, Variations in the progranulin gene affect global gene expression in frontotemporal lobar degeneration. *Hum. Mol. Genet.* **17**, 1349–1362 (2008). doi: 10.1093/hmg/ddn023; pmid: 18223198

30. J. B. Toledo *et al.*, A platform for discovery: The University of Pennsylvania Integrated Neurodegenerative Disease Biobank. *Alzheimers Dement.* **10**, 477–484.e1 (2014). doi: 10.1016/j.jalz.2013.06.003; pmid: 23978324

31. S. Andrews, FastQC: A Quality Control Tool for High Throughput Sequence Data (Java, 2010); https://www.bioinformatics.babraham.ac.uk/projects/fastqc/.

32. A. M. Bolger, M. Lohse, B. Usadel, Trimmomatic: A flexible trimmer for Illumina sequence data. *Bioinformatics* **30**, 2114–2120 (2014). doi: 10.1093/bioinformatics/btu170; pmid: 24695404

33. A. Dobin, T. R. Gingeras, in *Data Mining Techniques for the Life Sciences*, O. Carugo, F. Eisenhaber, Eds. (Springer, 2016), pp. 245–262.

34. B. van de Geijn, G. McVicker, Y. Gilad, J. K. Pritchard, WASP: Allele-specific software for robust molecular quantitative trait locus discovery. *Nat. Methods* **12**, 1061–1063 (2015). doi: 10.1038/nmeth.3582; pmid: 26366987

35. V. Obenchain *et al.*, VariantAnnotation: A Bioconductor package for exploration and annotation of genetic variants. *Bioinformatics* **30**, 2076–2078 (2014). doi: 10.1093/bioinformatics/btu168; pmid: 24681907

36. M. Carlson, TxDb.Hsapiens.UCSC.hg19.knownGene: Annotation package for TxDb object(s), R package version 3.2.2 (2015).

37. Y. Benjamini, Y. Hochberg, Controlling the False Discovery Rate: A Practical and Powerful Approach to Multiple Testing. *J. R. Stat. Soc. B* **57**, 289–300 (1995). doi: 10.1111/j.2517-6161.1995.tb02031.x

38. C. Wallace, Eliciting priors and relaxing the single causal variant assumption in colocalisation analyses. *PLOS Genet.* **16**, e1008720 (2020). doi: 10.1371/journal.pgen.1008720; pmid: 32310995

39. B. Liu, M. J. Gloudemans, A. S. Rao, E. Ingelsson, S. B. Montgomery, Abundant associations with gene expression complicate GWAS follow-up. *Nat. Genet.* **51**, 768–769 (2019). doi: 10.1038/s41588-019-0404-0; pmid: 31043754

40. R. Tian *et al.*, CRISPR Interference-Based Platform for Multimodal Genetic Screens in Human iPSC-Derived Neurons. *Neuron* **104**, 239–255.e12 (2019). doi: 10.1016/j.neuron.2019.07.014; pmid: 31422865

41. E. Danielson *et al.*, Molecular Diversity of Glutamatergic and GABAergic Synapses from Multiplexed Fluorescence Imaging. *eNeuro* **8**, ENEURO.0286-20.2020 (2020). doi: 10.1523/ENEURO.0286-20.2020; pmid: 33355295

42. B. R. Lee, T. Kamitani, Improved Immunodetection of Endogenous α-Synuclein. *PLOS One* **6**, e23939 (2011). doi: 10.1371/journal.pone.0023939; pmid: 21886844

43. P. Ewels, M. Magnusson, S. Lundin, M. Käller, MultiQC: Summarize analysis results for multiple tools and samples in a single report. *Bioinformatics* **32**, 3047–3048 (2016). doi: 10.1093/bioinformatics/btw354; pmid: 27312411

44. B. Li, C. N. Dewey, RSEM: Accurate transcript quantification from RNA-Seq data with or without a reference genome. *BMC Bioinformatics* **12**, 323 (2011). doi: 10.1186/1471-2105-12-323; pmid: 21816040

45. M. I. Love, W. Huber, S. Anders, Moderated estimation of fold change and dispersion for RNA-seq data with DESeq2. *Genome Biol.* **15**, 550 (2014). doi: 10.1186/s13059-014-0550-8; pmid: 25516281

46. A. Zhu, J. G. Ibrahim, M. I. Love, Heavy-tailed prior distributions for sequence count data: Removing the noise and preserving large differences. *Bioinformatics* **35**, 2084–2092 (2019). doi: 10.1093/bioinformatics/bty895; pmid: 30395178

47. K. Blighe, S. Rana, M. Lewis, EnhancedVolcano: Publication-ready volcano plots with enhanced colouring and labeling, Github (2021); https://github.com/kevinblighe/EnhancedVolcano.

48. P. S. T. Russo *et al.*, CEMiTool: A Bioconductor package for performing comprehensive modular co-expression analyses. *BMC Bioinformatics* **19**, 56 (2018). doi: 10.1186/s12859-018-2053-1; pmid: 29458351

49. P. Langfelder, B. Zhang, S. Horvath, Defining clusters from a hierarchical cluster tree: The Dynamic Tree Cut package for R. *Bioinformatics* **24**, 719–720 (2008). doi: 10.1093/bioinformatics/btm563; pmid: 18024473

50. A. Liberzon *et al.*, Molecular signatures database (MSigDB) 3.0. *Bioinformatics* **27**, 1739–1740 (2011). doi: 10.1093/bioinformatics/btr260; pmid: 21546393

51. G. Korotkevich *et al.*, Fast gene set enrichment analysis. *bioRxiv* 060012 (2021). https://doi.org/10.1101/060012.

52. H. Zigdon *et al.*, Identification of a Biomarker in Cerebrospinal Fluid for Neuronopathic Forms of Gaucher Disease. *PLOS One* **10**, e0120194 (2015). doi: 10.1371/journal.pone.0120194; pmid: 25775479

53. G. Kramer *et al.*, Elevation of glycoprotein nonmetastatic melanoma protein B in type 1 Gaucher disease patients and mouse models. *FEBS Open Bio* **6**, 902–913 (2016). doi: 10.1002/2211-5463.12078; pmid: 27642553

54. T. F. Tropea *et al.*, Whole Clinic Research Enrollment in Parkinson's Disease: The Molecular Integration in Neurological Diagnosis (MIND) Study. *J. Parkinsons Dis.* **11**, 757–765 (2021). doi: 10.3233/JPD-202406; pmid: 33492247

55. K. Pigott *et al.*, Longitudinal study of normal cognition in Parkinson disease. *Neurology* **85**, 1276–1282 (2015). doi: 10.1212/WNL.0000000000002001; pmid: 26362285

56. C. M. Lewis, Genetic association studies: Design, analysis and interpretation. *Brief. Bioinform.* **3**, 146–153 (2002). doi: 10.1093/bib/3.2.146; pmid: 12139434

SUPPLEMENTARY MATERIALS

science.org/doi/10.1126/science.abk0637
Materials and Methods
Figs. S1 to S7
Tables S1 to S12
MDAR Reproducibility Checklist
Data S1

View/request a protocol for this paper from *Bio-protocol*.

Science

GPNMB confers risk for Parkinson's disease through interaction with #-synuclein

Maria E. Diaz-OrtizYunji SeoMarijan PosaviMarc Carceles CordonElisia ClarkNimansha JainRakshita CharanMichael D. GallagherTravis L. UngerNoor AmariR. Tyler SkrinakRoseanne Davila-RiveraEliza M. BrodyNoah HanRebecca ZackVivianna M. Van DeerlinThomas F. TropeaKelvin C. LukEdward B. LeeDaniel WeintraubAlice S. Chen-Plotkin

Uncovering a contributor
Genome-wide association studies (GWAS) have uncovered nearly 100 loci that contribute to risk for Parkinson's disease (PD), which affects an estimated 6 million people worldwide. However, target genes and biological mechanisms associated with these loci remain largely unexplored. Diaz-Ortiz *et al.* examined a PD GWAS risk locus on chromosome 7, linking it to the transmembrane protein Glycoprotein Nonmetastatic Melanoma Protein B (GPNMB). GPNMB was found to interact with alpha-synuclein (aSyn), the key protein that forms the pathological inclusions that characterize PD (see the Perspective by Mollenhauer and von Arnim). In cells, GPNMB was both necessary and sufficient for the uptake of fibrillar forms of aSyn and the subsequent development of aSyn pathology. —SMH

View the article online
https://www.science.org/doi/10.1126/science.abk0637
Permissions
https://www.science.org/help/reprints-and-permissions

Use of this article is subject to the Terms of service